[SSC21-S1-28]

A Low-Voltage, Ultra-Compact Plasma Spectrometer for Small Spacecraft

Earl E. Scime
Department of Physics and Astronomy, West Virginia University
MS 6315, Morgantown, WV 26506; (304)293-5125
Escime@wvu.edu

Amy M. Keesee
Department of Physics and Astronomy and Space Science Center, University of New Hampshire
105 Main Street, Durham, NH 03824; (603)862-4316
amy.keesee@unh.edu

Matthew Dugas and Greg Wagner
Advanced Research Corporation
White Bear Lake, MN, USA; (651) 789-9000
gwagner@arcnano.com

ABSTRACT

Taking advantage of technological developments in wafer-scale processing over the past two decades, such as deep etching, 3-D chip stacking, and double-sided lithography, we have designed, fabricated, and tested the key elements of an ultracompact (1.7 cm-x 1.4 cm x 1.4 cm) plasma spectrometer that requires only low-voltage power supplies, has no microchannel plates, and has a high aperture area to instrument volume ratio. The energy analyzer and collimator components of the instrument are integrated into a single lithographically fabricated layer to optimize alignment of the collimator and eliminate flux reduction penalties typically associated with collimators. We will present tests of the instrument that demonstrate energy analysis of 5 keV electrons with only 5.3 volts of bias and collimator defined angular resolutions that match the design goals of the instrument.

INTRODUCTION

Beginning with single spacecraft and progressing to multi-spacecraft missions, exploration of near-Earth space has increasingly focused on understanding the energy flow and coupling between different spatial regions through simultaneous measurements of plasma parameters, e.g., magnetic field, electric field, density, and temperature. The International Solar Terrestrial Physics (ISTP) program's Wind, Polar, and Geotail missions[1,2] and the THEMIS mission[3] provided new insights and global perspectives on the flow of energy from the solar wind through the magnetosphere. Though highly successful, those missions were, and continue to be, limited by rare conjunctions, and simultaneous sampling of only a few widely separated locations. The Magnetosphere Multiscale Mission (MMS) has separations down to 10 km and the spacecraft fly in an approximately tetrahedral configuration[4] (as does the Cluster mission);[5] enabling direct calculations of the curl of the magnetic field and other 3D spatial differential quantities. Such spatially resolved measurements are critical for understanding the electrodynamics of the magnetosphere, but they provide limited information about the instantaneous global state of the magnetosphere.

The next step in multi-spacecraft missions is to go well beyond missions consisting of a handful of large and sophisticated spacecraft to missions comprised of large numbers of simple micro or pico-spacecraft. Only by flying 100s of spacecraft and thereby obtaining simultaneous, high spatial resolution plasma measurements over a significant fraction of the entire magnetosphere will it be possible to understand the energy flow and coupling between different magnetospheric regions. However, the current generation of plasma spectrometers are too massive, consume too much electrical power, and require too much assembly and testing time to be flown on future multi-spacecraft microsatellite missions. Advanced wafer scale fabrication techniques naturally lend themselves to relatively high manufacturing volumes, lower mass, lower costs, and therefore change the paradigm for dealing with flaws or defects in individual instruments. Before describing the wafer-based plasma

instrument concept, it is useful to briefly review the features of a typical spacecraft plasma instrument.

A classic plasma instrument, e.g., the "top hat" analyzer,[6] consists of a collimator followed by an energy per charge resolving spectrometer followed by a detector. For collimation, a conventional plasma spectrometer employs either a grounded or an electrically biased collimating structure to sweep out unwanted charged particles while narrowing the field of view for the desired particles (charged or neutral). To reduce the effects of sunlight on the detectors, the energy resolving spectrometer typically introduces a significant path deflection for charged particles but not for light. In other words, photons entering the instrument meet some physical obstruction while the desired charged particles are electrostatically guided around the obstruction to the detector. The third element in a conventional plasma instrument is the detector. Low to medium energy (1 eV to 40 keV) instruments from thirty years ago relied on discrete channel electron multipliers for particle detection.[7] Designers of modern instruments have switched to microchannel plates (MCPs) because of their larger detection areas, comparable sensitivities, and considerably improved spatial resolution. However, MCPs must be carefully outgassed before use,[8] require relatively high voltages for biasing,[9] and experience continual degradation over the life of a nominal space mission.[10,11] Higher energy plasma instruments (for energies greater than 40 keV) use solid state detectors for both particle detection and energy measurement. Advances in silicon solid state detector (SSSD) fabrication have reduced the energy threshold for such detectors to a few keV.[12,13] Therefore, a medium to high energy plasma instrument could conceivably employ a solid state detector and eliminate the need for MCPs.

It is the energy per charge spectrometer that forces a trade-off in mass, volume, and sensitivity. *Zerbuchen and Gershman's* analysis of space plasma instrument technology noted that when the sensitivity of plasma instruments scales with R^2 or faster, where R is the characteristic radius of the energy spectrometer, electric fields in the sensors become too large for small characteristic radii.[14] The instrument development effort described here breaks the historic R^2 scaling of plasma instrument sensitivity while also eliminating the problems associated with increasingly large electric fields in small instruments and separate collimating structures.

Miniaturization of plasma instruments has proceeded along two paths. Conventional "top-hat" style instruments have been miniaturized, e.g. the Thermal Electron Capped Hemispherical Spectrometer instrument,[15] and flown in cold, high density, space plasma environments suitable for their small sensitivities and low energy passband. The small sensitivity arises from the reduced instrument size (the R^2 scaling of the curved plate electrostatic analyzer noted previously) and the low energy passband results from the need to keep electric fields created by the hemispherical electrostatic plates in the instrument below thresholds for arcing. Even miniaturized, those instruments still require high voltages, many kV, to operate their MCPs.

The other approach to miniaturization has been to develop multi-layer, micro-machined structures that accomplish energy selection without curved electrostatic plates for photon suppression. For example, the Flat Plasma Spectrometer (FlaPS) employed straight micromachined channels to deflect ions of energies up to 50 keV past a blocking mask.[16] The channels were fabricated with micro electrical discharge machining. In laboratory tests, a bias voltage of approximately 10 keV was required to direct a 20 keV ion to the detector. The same basic instrument concept was incorporated into the WISPERS plasma instrument, launched in 2010 on the FalconSat-5 spacecraft. The FlaPS analyzer concept has an energy selection scaling of $(L/\Delta X)^2$. For the plate length (L) of 1 mm and plate spacing (ΔX) of 300 μm used in WISPERS, the predicted differential voltage of 13,600 V needed to deflect a 20 keV singly charged ion around the light blocking baffle at the exit plane is consistent with their laboratory tests.[16] Since the target ionospheric plasmas for the WISPERS mission were very cold, temperatures less than a few eV, an instrument power supply of only 10 V was sufficient to provide WISPERS with a scientifically useful energy range of 0 to 25 eV. However, for magnetospheric and heliospheric ions at energies of 10's of keV, a FlaPS-type energy analyzer would require many kV bias voltages.

For a curved plate analyzer at a fixed bias voltage difference, the energy of transmitted charged particles is $E = q\Delta V 2\ln(1+\Delta r/R_1)$, where R_1 is the inner plate radius and Δr is the plate spacing. For closely spaced plates, the transiting energy reduces to $E = qR\Delta V 2\Delta r$ to first order, i.e., the energy scales with the average radius of the analyzer divided by twice the plate spacing. The focusing properties of a cylindrical curved plate analyzer are optimal for a bending angle of 127°.[17] At this angle, charged particles injected at the center of the analyzer plates but with a wide range of incident angles successfully pass through the analyzer and are focused upon exiting. For a spherical or "top hot" analyzer, the optics are different. A smaller bending angle is used and two-dimensional electrostatic focusing is sacrificed so that a fully two dimensional

aperture is achieved, which improves the geometric factor of the instrument. Conventional manufacturing constraints, and the need to maximize the size of the input aperture, set the scale of the spacing between the curved plates. In the hemispherical analyzer of *Young et al.*,[6] the plate spacing was 0.5 cm and a differential voltage of 2,350 V was required to convey 20 keV ions to the detector. When top hat analyzers are miniaturized, either the required bias voltage must increase if large plate spacing, and therefore the geometric factor, is to be preserved, or the plate spacing must shrink at the expense of the geometric factor (sensitivity).

Here we describe initial test results of an ultra-compact, plasma energy analyzer developed for flight on microsatellites. A key feature of the instrument concept is the use of hundreds of apertures in parallel to increase the sensitivity (geometric factor) of the instrument. The instrument is comprised of 25 layers, with each layer comprised of 8 energy resolving bands. Each band is comprised of 10 parallel curved plate analyzers. Bias voltages are applied to the individual curved plate analyzers through a resistive voltage divider network. The 25 bands in each vertical column in the instrument operate in parallel. Thus, the instrument can sample eight different energies simultaneously. The layer-to-layer electric connections are accomplished by "through-substrate-via" technology (TSV), the same method used in the semiconductor industry to produce multilayer processors.

The core elements of the instrument are fabricated using conventional chip manufacturing techniques (photomasking, thin film deposition, and etching) and are easily scaled to large production volumes. In the complete instrument, the spectrometer will be mated to a silicon solid state detector with a detection threshold on the order of 1 keV. The initial designs of this instrument concept relied on separately fabricated collimator and energy analyzer (EA) elements etched into highly-conductive silicon.[4] The next generation version of the instrument, described here, includes a collimating structure that is integrated into each energy analyzer layer.

SINGLE LAYER FABRICATION

The prototype combined Collimator and Energy Analyzer (CEA) layers ("chips") were designed with several straight bands to be used as fiducials in testing, as shown in Figure 1. Every CEA includes eight bands that each have a collimator section (top) mechanically and electrically isolated from the EA section (bottom). Each collimator band consists of 10 straight channels (80 µm wide) created by 9 fins (60 µm wide) that are tapered at the entrance. The EA section of the prototype CEA includes four curved bands (bands 3, 4, 6, and 7 as numbered from the left of Figure 1). Band 1 contains no fins. Bands 2, 5, and 8 contain straight channels. All channels in the lower portion (except for band 1) have the same channel and fin width as the collimator section. The overall dimensions of the CEA shown in Figure 1 are 1.8 cm wide, 1.5 cm high, and 0.15 cm thick. A CEA for implementation would have all eight EA bands curved with varying bias voltages applied to obtain an energy spectrum.

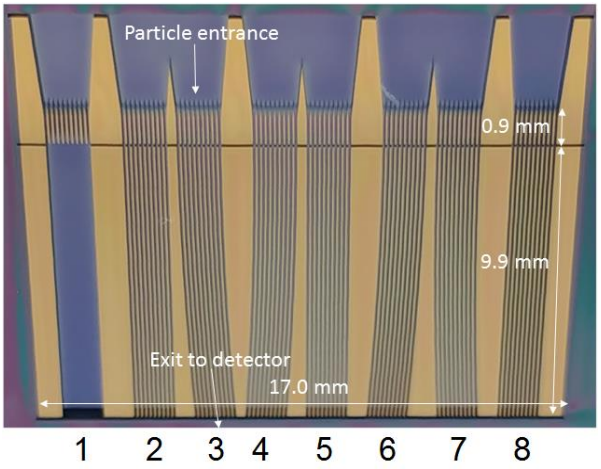

Figure 1. White light image of a complete CEA. The collimator is at the top. Eight bands, numbered from the left, include one straight with no fins (1), three straight (2, 5, 8), and four curved (3, 4, 6, and 7) EA bands. Adapted with permission from Fig. 1 of Keesee et al., Rev. Sci. Instrum. 89, 10J116 (2018). Copyright 2018 AIP.

The CEA chips were fabricated using a proprietary Deep Reactive Ion Etching (DRIE) recipe.[5] Shown in Figure 2a is a scanning electron microscope (SEM) image of the entrance region of the collimator section. The collimator fins are tapered to reduce scattering from the corners and to tune the angular acceptance of the collimator to the desired ± 2.5º angular field-of-view. Particles enter from the top in Figure 1, travel through the collimator for angular selection, then through the curved energy analyzer channels for energy selection, then out the bottom of Figure 1 to a detector. Shown in Figure 2b is an SEM image of the junction between the collimator structure and the EA. The collimator fins are mechanically and electrically isolated from the energy analyzer fins. The well-defined, high aspect ratio, vertical side walls of the fins produced by the DRIE fabrication process are evident. As designed, each fin is 360 µm tall and 60 µm wide. The gap between the fins is 80 µm. The fins are fabricated in highly conductive silicon layer bonded to

a glass substrate. The silicon layer has an electrical conductivity comparable to aluminum.

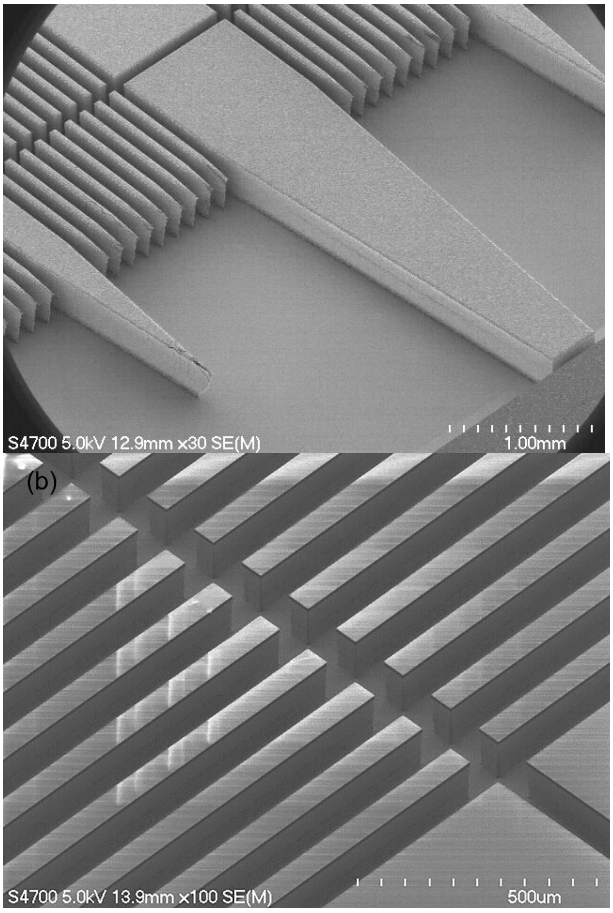

Figure 2. (a) Scanning electron microscope (SEM) image of the collimator entrance. (b) SEM image showing the mechanical separation between the collimator and EA sections of the CEA.

Biasing of the fins is accomplished with a conductive layer lithographically deposited on the underside the glass substrate (using conventional double-side lithography). This conductive layer has the same pattern as the CEA in the EA region, but the collimator region of the electrical interconnect layer is a continuous conductive plane to provide for grounding of the collimator fins. Instead of making electrical connections to each individual fin, the underside layer includes a thin strip of deposited resistive boron-hydride aligned perpendicularly to the fins as a voltage divider. The thickness and width of the boron-hydride strip is tuned to obtain fin-to-fin electrical resistances in the few hundred kilohm range after bonding. Thus, when bias voltages are applied between the large pads on either side of each band (see Figure 1), the overall bias current is only a few microamps. Direct fin connections were used to confirm that the boron-hydride voltage divider functions as intended.

For initial single layer testing, a single CEA was bonded to a biasing layer deposited onto a glass substrate and the entire structure placed in an enclosure and illuminated with a high-uniformity, 5 keV electron beam in the space plasma calibration laboratory at Goddard Space Flight Center. An imaging microchannel plate (MCP) detector was placed behind the CEA to record the flux of electrons passing through the CEA. The enclosure included a series of baffles and slits to restrict the transiting electrons to only those that passed through the CEA. The angle of the instrument aperture relative to the beam direction could be varied in both pitch and azimuth. Electrical connections to the instrument were made via a multi-pin vacuum feedthrough.

SINGLE LAYER TESTING

As shown in Figure 3, we have successfully demonstrated that the CEA selectively allows passage of 5 keV electrons through the curved channels for an applied bias of only a few tens of volts. Figure 3 shows the two-dimensional image of detected electron flux through straight bands 1, 5, and 8, along with flux through curved bands 6 and 7 for a -60 V bias voltage applied to those two bands. All other pads, between the bands, were connected to ground. Shown in Figure 4 are one-dimensional profiles of total flux measured in seven detector rows (a seven-pixel high horizontal cut through Figure 3) as a function of detector columns. In Figure 4a, with 0 V applied, electrons are detected only through straight bands 1, 5, and 8. The intensity from band 1 is significantly larger due to the lack of fins in the EA section (allowing transmission of greater flux through that band). In Figures 4b (-40 V) and 4c (-54 V), flux from bands 6 and 7 is apparent with varying intensities depending on applied voltage. Note that these peaks occur on the outside of the peaks for bands 5 and 8, indicating that, as expected, the curved channels of bands 6 and 7 divert the electrons such that they cross paths with those emanating from the straight channels of bands 5 and 8. The curved EA channels have a radius of curvature of 150 mm and a length of 9.930 mm, diverting the electrons by an angle of 3.8°. The detector is mounted approximately 64 mm behind the CEA. Thus, the electrons will travel approximately 4.2 mm transverse to the detector normal, which is equivalent to 24 pixels on the detector. This is consistent with the observations in Figure 4b and 4c in which the peaks from bands 6 and 7 appear shifted ~20 pixels from the detector regions directly in front of those bands.

An important feature of the CEA is that since the collimator fins are completely aligned with the EA fins, the effective transparency of the collimator fins is 100%. The result is a peak transmitted flux through the

curved bands that equals or exceeds the flux through the straight fins (Figure 4c). Typically, the transparency of the collimator is an additional loss term in the overall transmitted flux for an energy analyzer. The flux through the curved bands 6 and 7 exceeding the flux through the straight bands 5 and 8 is likely a result of the intrinsic beam divergence of the calibration beam.

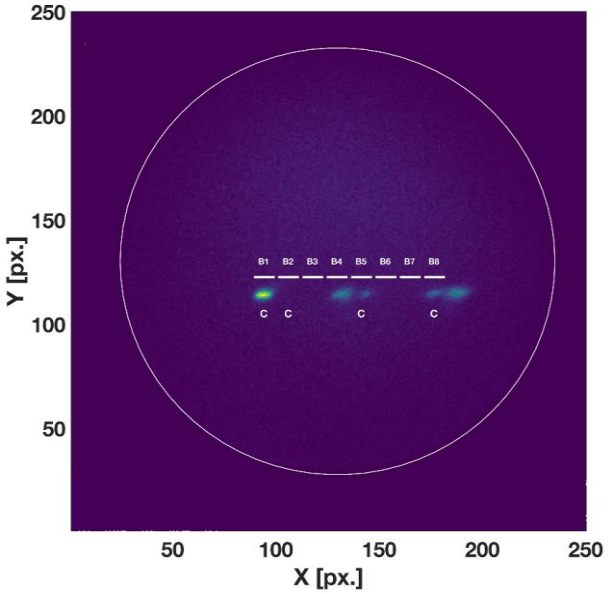

Figure 3. Two dimensional MCP image of detected counts for an applied bias of -60 V across bands 6 and 7. Signal is detected from collimator-only (indicated with a C) bands 1, 5, and 8 and EA bands 6 and 7. Adapted with permission from Fig. 3 of Keesee et al., Rev. Sci. Instrum. 89, 10J116 (2018). Copyright 2018 AIP

During testing it was observed that maximum flux through bands 5 and 8 occurred for rotation angles of the CEA in the beam that differed by less than 0.2º (the collimator angular acceptance is smaller than the electron beam divergence). For the measurements shown in Figure 4, the CEA was rotated to an angle in between the peak transmitted flux angles for bands 5 and 8, thereby optimizing the alignment of bands 6 and 7 with the calibration beam. This beam divergence effect is also why little to no flux appears behind straight band 2 in Figure 4.

The overall energy resolution of band 6 was investigated by measuring the transmitted flux as a function of applied bias voltage. For 5 keV electrons, Δr = 80 µm, and R = 150 mm, the required voltage difference across each channel is V = -5.33 V. To obtain that voltage across each channel, a bias of -53.3 V is needed across the entire band of 10 channels. Figure 5 shows the transmitted flux as a function of applied bias

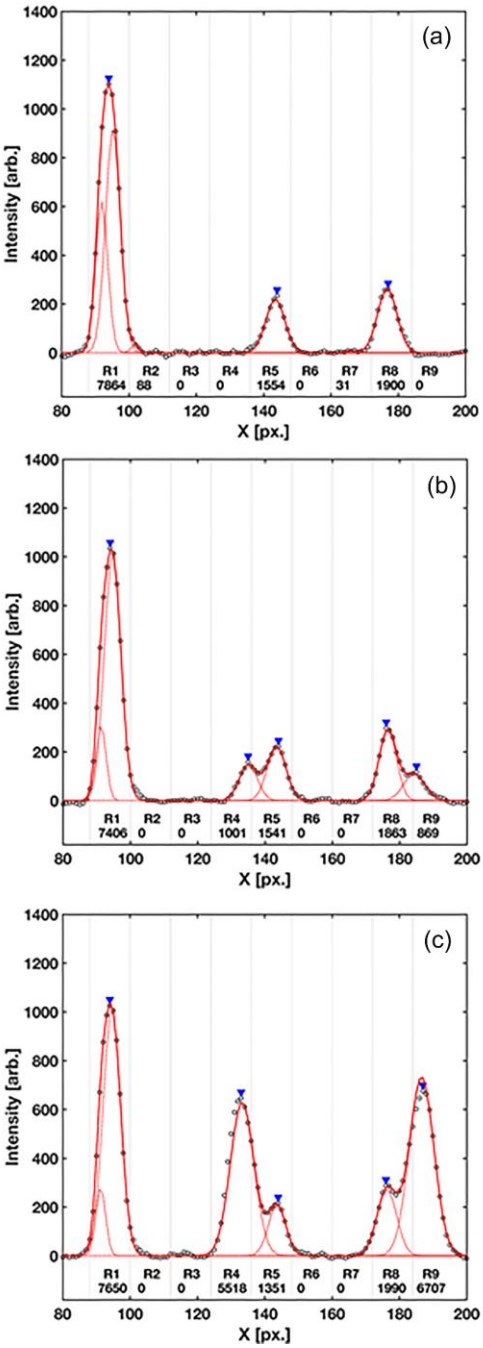

Figure 4. Profiles of electron flux versus pixel location for an applied voltage of (a) 0 V, (b) -40 V, and (c) -54 V. The data are shown as black circles, a multi-Gaussian fit is shown as a dashed red line, and the total of the fits is shown as a solid red line. Blue triangles indicate the location of the fit peaks. The detector is divided into nine regions (R1-R9) and the total flux in each region is shown below the label. Adapted with permission from Fig. 4 of Keesee et al., Rev. Sci. Instrum. 89, 10J116 (2018). Copyright 2018 AIP

voltage for band 6. The peak in signal is exactly at the expected applied voltage of -53 V.

As noted previously, an ideal curved plate electrostatic analyzer would have curved fins that subtend an angle of 127º to obtain first-order focusing of charged particles at the image (detector) plane. The CEA developed here subtends a much smaller angle (just enough to require photons to make a single bounce to pass through the instrument). Therefore, the energy resolution of this instrument is expected to be much worse than the nominal energy resolution of $\Delta E/E \sim \Delta r/R$ for an ideal curved plate analyzer, where ΔE is half the full width of the transmission function. The half width at half maximum (HWHM) of the measurements shown in Figure 5 is $\Delta V/V = 7\%$. The energy resolution could be improved by increasing the angle subtended by the curved fins as the expense of a more complicated geometry at the exit plane of the instrument.

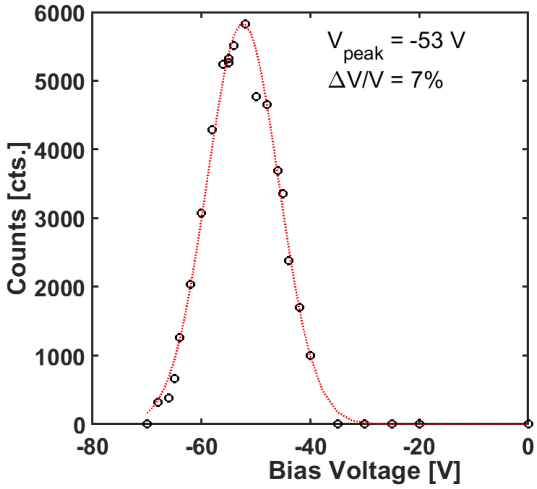

Figure 5. Measured counts from band 6 as a function of applied voltage across band 6. Adapted with permission from Fig. 5 of Keesee et al., Rev. Sci. Instrum. 89, 10J116 (2018). Copyright 2018 AIP

To validate the angular resolution of the instrument, the CEA assembly was scanned in azimuth (along the *X* direction in Figure 3) to determine the angular acceptance of the bands (around the orientation angle for peak transmitted flux). Flux as a function of azimuthal angle for bands 1 and 8 is shown in Figure 6. Band 1 consists of only the collimator section designed to provide the desired angular acceptance, given by

$$\tan(\theta) = (\Delta r/2L) \quad (1)$$

where Δr is the channel spacing and L is the length of the short collimator section. For the spacing of $\Delta r = 80$ µm, the collimator was designed to have $L = 0.914$ mm to yield an angular acceptance of ± 2.5°. The measurements shown in Figure 6a are a superposition of the flux through bands 1 and 2. The total flux is dominated by the much greater intensity of band 1. Thus, it is asymmetric and not well fit by a Gaussian distribution. However, the FWHM of the fit of 3.6° and acceptance cutoff of ± 3° (considering the non-zero intensity between -4° and 2° in azimuth) indicate an angular acceptance only 0.5°-1.0° larger than the prediction. The electron source size and electron beam divergence cause the measured acceptance angle to be larger than the expected value.

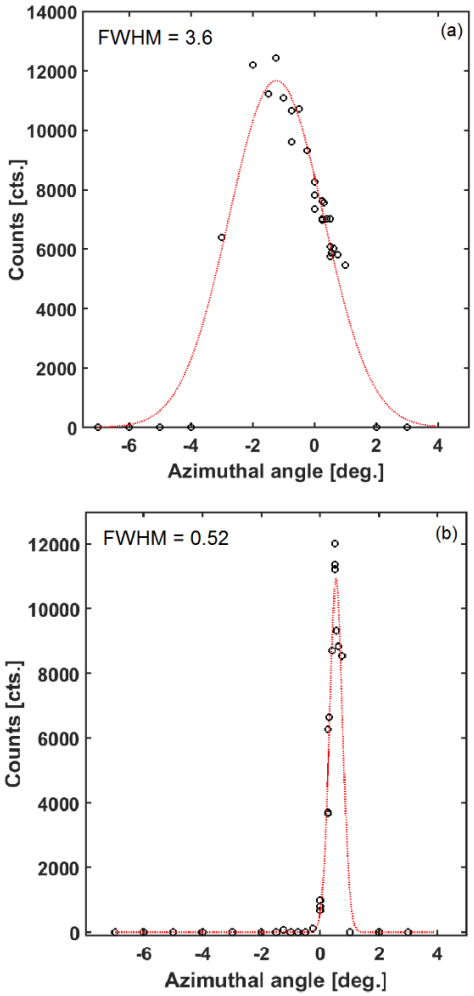

Figure 6. Measured flux from (a) band 1 and (b) band 8 as a function of azimuthal angle. Adapted with permission from Fig. 6 of Keesee et al., Rev. Sci. Instrum. 89, 10J116 (2018). Copyright 2018 AIP

The longer channels of the straight bands (collimator and EA combined) have $L = 10.844$ mm, yielding an expected angular acceptance of ± 0.4°. The measured angular acceptance (Figure 6b) with a FWHM = 0.52° is slightly larger than expected, but it agrees with theoretical predictions based on the electron source size

and beam divergence. In addition to the beam characteristics, the backlash in the angular positioning system during the measurements was observed to be on the order of 0.2°, therefore the measured FWHM has an uncertainty larger than the difference in the predicted and measured values. The backlash in the positioning system was only discovered because of the extremely high angular resolution of the CEA assembly. No previous instruments tested in the facility had ever had angular resolutions so small.

A limited scan in pitch angle (along the *Y* direction in Figure 3) was performed. Preliminary results indicated an angular acceptance similar to that seen in Figure 6b. However, we would expect a larger angular acceptance in this dimension since the channels are taller than they are wide (360 µm vs. 80 µm). We hypothesize that the entrance aperture on the housing limited the angular acceptance in this dimension. The tall channels were used to ensure adequate signal for these initial tests. The final instrument would likely have square channels to provide similar spatial resolution in both dimensions.

FIVE LAYER STACK

Shown in Figure 7a is a CAD rendering of a 5-layer stack along with the electrical readout layer at the top of the stack. Shown in Figure 7b is a photograph of stack of five identical CEA layers, each with the double-side lithography needed to create the electrical connections between the layers. This five stack was manufactured using the complete fabrication process including TSV interconnects through each layer, the double-sided lithography, indium and silver deposition on the ESA fins and electrical connection layer, and deposition of the boron-hydride resistor. Final electrical connections will be made at the top of the stack with a capping layer and the biasing connections feed out through a single ribbon cable at the top of the stack.

Probe measurements confirm that each of the eight bands in the vertical columns in the stack are biased properly and the individual fins are biased through the voltage dividers as expected. The overall dimensions of the five layer stack are 1.4 cm x 1.7 cm x 0.28 cm. Thus, a full twenty-five layer stack (1.4 cm high) would easily fit on a microsatellite. As shown in previous work,[16] the 2000 parallel apertures of a twenty-five layer instrument result in a geometric factor comparable to a conventional plasma spectrometer. The geometric factor of this instrument scales linearly (not quadratically) with instrument size, i.e., a row of ten of these instruments (17 cm x 1.4 cm x 1.4 cm) would have ten times the geometric factor.

CONCLUSIONS

We have successfully fabricated and tested key components of a miniature energy analyzer instrument capable of energy analysis of few eV to keV ions and electrons using applied voltages that are a small fraction of the particle energy. The instrument is capable of sampling eight different energies simultaneously. The 7% energy resolution of the instrument is sufficient to provide excellent energy selectivity for any desired energy range. The entire instrument is compact enough to fly on a microsatellite. With a simple solid state detector, such an instrument would not require any high voltage power supplies and is ideally suited for mass manufacturing. With an energy-resolving detector, energy measurements in the detector could be used for anti-coincidence detection given the known instrument energy passband. Such an anti-coincidence detection scheme would facilitate rejection of light contamination and signals from penetrating radiation.

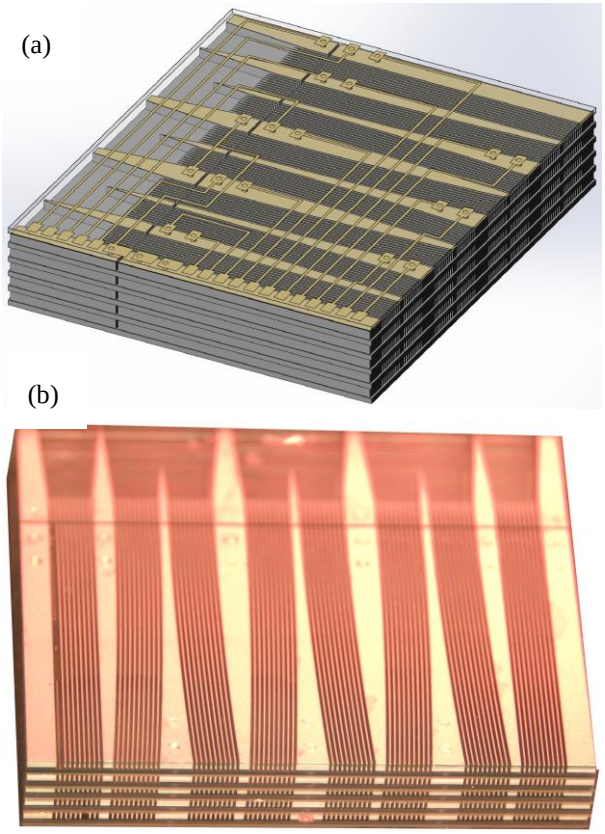

Figure 7. (a) CAD rendering of a complete 5-layer CEA stack with a specialized electrical connector top layer. (b) Photograph of a 5-layer stack.

ACKNOWLEDGMENTS

This work supported by NASA Award 80NSSC19K0490.

REFERENCES

1. M. Desch, K. Ogilvie, M. Acuna, D. Fairfield, and R. Hoffman, "Early Multiplatform Results from the International Solar Terrestrial Physics/Global Geospace Science (ISTP/GGS) Program," Geophys. Res. Lett., vol. 24, 913, 1997.

2. T I. Pulkkinen, D. N. Baker, Niescja E. Turner, H J. Singer, L A. Frank, "Solar Wind-Magnetosphere Coupling During an Isolated Substorm Event: A Multispacecraft ISTP Study," Geophys. Res. Lett., vol. 24, 983, 1997.

3. V. Angelopoulos, "The THEMIS Mission," Space Science Reviews, vol. 141, 5–34, doi:10.1007/s11214-008-9336-1, 2008.

4. Burch, J.L., T.E. Moore, R.B. Torbert, B.L. Giles, "Magnetospheric Multiscale Overview and Science Objectives," Space Sci Rev., vol. 199:5–21 DOI 10.1007/s11214-015-0164-9, 2016.

5. Escoubet, C.P., Fehringer, M., Goldstein, M.**,** **"**The Cluster mission," Annales Geophysicae, vol. 19, 1197-200, 2001.

6. Young, D.T., S.J. Bame, M.F. Thomsen, R.H. Martin, J.L. Burch, J.A. Marshall, B. Reinhard, "2π-radian field-of-view toroidal electrostatic analyzer," Rev. Sci. Instrum. 59, 743-51, 1988.

7. Bame, S.J., D.J. McComas, B.L. Barraclough, J.L. Phillips, K.J. Sofaly, J.C. Chavez, B. E. Goldstein, R.K. Sakurai, "The Ulysses solar wind plasma experiment," Astron. Astrophys. Suppl. Series 92, 237-65, 1992.

8. Siegmund, O.H.W. et al., "Atomic layer deposited borosilicate glass microchannel plates for large area event counting detectors," Nucl. Instrum. Meth. A 695, 168, 1992.

9. Lin, R.P., K.A. Anderson, S. Ashford, C. Carlson, D. Curtis, R. Ergun, D. Larson, J. McFadden, M. McCarthy, G.K. Parks, H. Reme, J.M. Bosqued, J. Coutelier, E. Cotin, C. D'Uston, K.-P. Wenzel, T.R. Sanderson, J. Henrion, J.C. Ronnet, G. Paschmann, "A Three-Dimensional Plasma and Energetic Particle Investigation for the Wind Spacecraft," Space Sci. Rev., vol. 71, 125-53, 1995.

10. Kataria, D.O., G. Watson, P.J. Carter, A.N. Fazakerley, A.M. James, R.J. Wilson, "In-flight monitoring and optimization of MCP performance of multi-spacecraft missions, Low-Light-Level and Real-Time Imaging Systems, Components, and Applications," Proceedings of the SPIE - The International Society for Optical Engineering, 4796, 115-25, 2003.

11. Kishimoto, N., M. Nagamine, K. Inami, Y. Enari, and T. Ohshima, "Lifetime of MCP-PMT," Nucl. Instrum. Methods Phys. Res. A, vol. 564, 204, 2006.

12. Tindall, C.S., N.P. Palaio, B.A. Ludewigt, S.E. Holland, D.E. Larson, D.W. Curtis, S.E. McBride, T. Moreau, R.P. Lin, V. Angelopoulos, "Silicon Detectors for Low Energy Particle Detection," IEEE Transactions Nucl. Sci., vol. 55, 797, 2008.

13. Ogasawara, K., F. Allegrini, M. I. Desai, S. Livi, and D. J. McComas, "A Linear Mode Avalanche Photodiode for Ion Detection in the Energy Range 5–250 keV," IEEE Transactions on Nuclear Science, vol. 59, 2601, 2012.

14. Zurbuchen, T.H. and D.J. Gershman, "Innovations in Plasma Sensors," J. Geophys. Res., vol. 121, 2891, doi:10.1002/2016JA022493, 2016.

15. Pollock, C., V. Coffey, J. England, N. Martinez, T. Moore, and M. Adrian, Thermal electron capped hemisphere spectrometer, TECHS) for ionospheric studies, in Measurement Techniques in Space Plasmas: Particles, pp. 201–207, American Geophysical Union, 1998.

16. Wesolek, D. M., F.A. Hererro, R. Osiander, M.A.G. Darrin, "Design, fabrication, and performance of a micromachined plasma spectrometer," J. Microlith. Microfab. Microsys., vol. 4, 41403, 2005.

17. Hughes A. LL. and V. Rojansky, "On the Analysis of Electronic Velocities by Electrostatic Means," Phys. Rev., vol. 34, 284, 1929.

18. E. E. Scime, A. Barrie, M. Dugas, D. Elliott, S. Ellison, A. M. Keesee, C. J. Pollock, A. Rager, and J. Tersteeg, "Key elements of a low voltage, ultracompact plasma spectrometer," J. Geophys. Res. Space Physics, vol. 121, 1452–1465, 2016. doi:10.1002/2015JA022208.

19. Yeom, J., Wu, Y., Selby, J. C., & Shannon, M. A., "Maximum achievable aspect ratio in deep reactive ion etching of silicon due to aspect ratio dependent transport and the microloading effect," Journal of Vacuum Science & Technology B: Microelectronics and Nanometer Structures, vol. 23(6), 2319, 2005. http://doi.org/10.1116/1.2101678